ChemComm

COMMUNICATION

View Article Online
View Journal | View Issue

Cite this: *Chem. Commun.*, 2018, **54**, 1533

Received 2nd November 2017,
Accepted 11th January 2018

DOI: 10.1039/c7cc08423d

rsc.li/chemcomm

$CoC_2O_4{\cdot}2H_2O$ derived Co_3O_4 nanorods array: a high-efficiency 1D electrocatalyst for alkaline oxygen evolution reaction†

Yicheng Wei, Xiang Ren, Hongmin Ma, Xu Sun, Yong Zhang, Xuan Kuang, Tao Yan, Huangxian Ju, Dan Wu* and Qin Wei

Energy conversion and storage systems such as water splitting metal–air batteries require high-performance and durable oxygen evolution reaction (OER) catalysts. Herein, we report the *in situ* development of self-standing Co_3O_4 nanorods array on Co foil (Co_3O_4 NA/CF) as a 1D OER catalyst electrode. Such Co_3O_4 NA/CF only needs overpotential of 308 mV to drive a geometrical catalytic current density of 15 mA cm^{-2} in 1.0 M KOH with good long-term electrochemical durability. In addition, this catalyst achieves a high turnover frequency of 0.646 mol O_2 s^{-1} at overpotential of 410 mV.

Rising energy demands and environmental consequences have triggered plenty of research on clean and sustainable energy systems.[1] Hydrogen is considered as an ideal candidate for high energy output and carbon-neutral combustion products.[2,3] Electrocatalytic water splitting is a promising technology for large-scale production of hydrogen. However, the oxygen evolution reaction (OER) is identified as having sluggish kinetics because it requires a multi-electron transfer process, which builds up very high potentials.[4,5] Currently, RuO_2 and IrO_2 are the best OER catalysts, but low abundance and high cost significantly hinder their large-scale commercial applications.[6] Therefore, it is highly necessary to develop efficient and earth-abundant OER catalysts.

Co has emerged as an interesting non-noble metal with catalytic power towards water oxidation and a variety of Co-containing materials have been explored as OER catalysts.[7–10] Among them, spinel-type Co_3O_4 with good conductivity has been proven as an excellent and energy-efficient OER catalyst. Recently, various structures of Co-containing solid precursors have been developed to derive Co_3O_4, such as cobalt hydroxide, cobalt nitrate hydroxide, cobalt phosphate, cobalt nitrate carbonate hydroxide, cobalt hydroxy oxide, cobalt oxalate, cobalt carbonate, and Co-based metal–organic frameworks.[11–19] Notably, the assembly of the precursors involve a high-temperature process and thus, it is rather energy-intensive. Moreover, the synthesis of a 1D nanostructure with a multicomponent surface is highly desired to achieve high catalytic performance.[20–24] Hence, room-temperature fabrication of 1D Co-containing solid precursors to derive Co_3O_4 for highly efficient and durable OER is highly desired.

In this communication, we report our recent effort toward the development of self-standing Co_3O_4 nanorods array on Co foil (Co_3O_4 NA/CF) *via* room-temperature *in situ* electrochemical preparation of $CoC_2O_4{\cdot}2H_2O$, followed by thermal decomposition (Scheme 1, see ESI† for preparation details). Such 1D Co_3O_4 NA/CF behaves as a superior oxygen-evolving catalyst electrode and only requires overpotential as low as 308 mV to drive a geometrical catalytic current density of 15 mA cm^{-2} in 1.0 M KOH, thus outperforming most reported Co_3O_4-based catalysts. Notably, it also demonstrates good long-term electrochemical durability for at least 22 h. Moreover, this catalyst achieves a high turnover frequency (TOF) of 0.646 mol O_2 s^{-1} at an overpotential of 410 mV.

Fig. 1a shows the X-ray diffraction (XRD) patterns for $CoC_2O_4{\cdot}2H_2O$ NA/CF and Co_3O_4 NA/CF. $CoC_2O_4{\cdot}2H_2O$ NA/CF shows diffraction peaks at 18.7°, 22.7°, 24.8°, 29.2°, 30.2°, 35.1°, 41.8°, and 44.5° that can be indexed to the (202), (004), (113), (114), (313), (022), (511), and (117) planes of $CoC_2O_4{\cdot}2H_2O$ phase, respectively (JCPDS No. 25-0250).[25] After thermal decomposition, the resultant Co_3O_4 NA/CF also presents characteristic

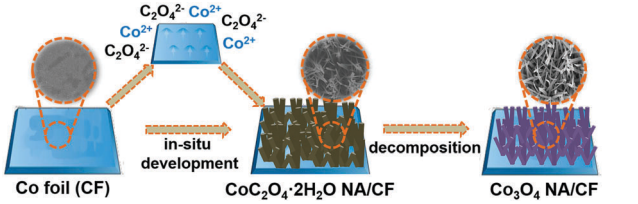

Scheme 1 A schematic diagram to illustrate the two-step fabrication of Co_3O_4 NA/CF.

Key Laboratory of Interfacial Reaction & Sensing Analysis in Universities of Shandong, School of Chemistry and Chemical Engineering, University of Jinan, Jinan 250022, Shandong, China. E-mail: wudan791108@163.com

† Electronic supplementary information (ESI) available: Experimental section and supplementary figures. See DOI: 10.1039/c7cc08423d

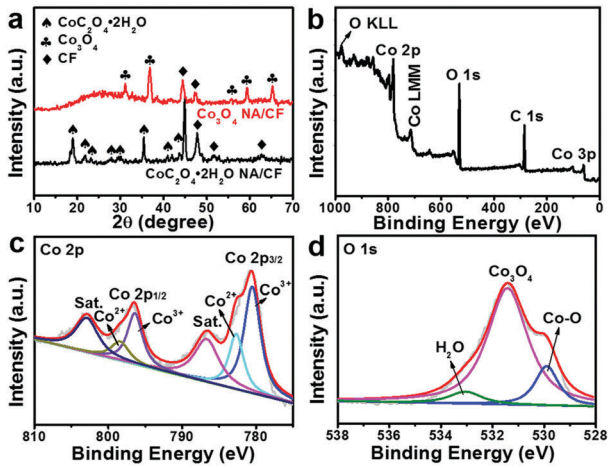

Fig. 1 (a) XRD patterns for $CoC_2O_4·2H_2O$ NA/CF and Co_3O_4 NA/CF. (b) XPS survey spectrum for Co_3O_4. XPS spectra of Co_3O_4 in the (c) Co 2p and (d) O 1s region.

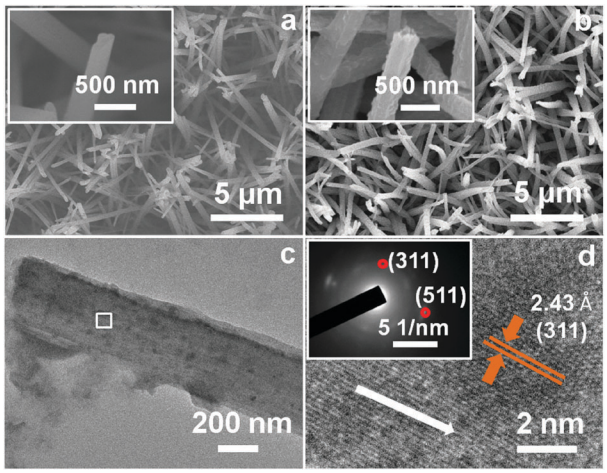

Fig. 2 SEM images for (a) $CoC_2O_4·2H_2O$ NA/CF and (b) Co_3O_4 NA/CF. (c) TEM and (d) HRTEM image for Co_3O_4 (inset: SAED pattern).

peaks at 31.3°, 38.5°, 55.6°, 59.4°, and 65.2°, indexed to the (220), (311), (422), (511), and (440) planes of Co_3O_4, respectively (JCPDS No. 42-1467).[25] Fig. 1b shows the X-ray photoelectron spectroscopy (XPS) survey of Co_3O_4, further confirming the presence of Co and O elements. The Co 2p spectrum shown in Fig. 1c could be divided into six peaks, which are assigned to $2p_{3/2}$ of Co^{2+} (782.3 eV) and Co^{3+} (780.5 eV) ions, $2p_{1/2}$ of Co^{2+} (798.5 eV) and Co^{3+} (796.4 eV) ions, as well as the corresponding satellite peaks (identified as "Sat.") at 786.5 and 802.9 eV that arise from Co^{2+}. The relative atomic ratio of Co^{2+}/Co^{3+} (1.2/2.5) on the surface of Co_3O_4 could be obtained by comparing the area that the fitted curve.[26,27] In addition, the O 1s (Fig. 1d) peak at 531.4 eV is the typical metal–oxygen (Co_3O_4) bond, and two weak shoulders attribute to oxidation of Co surface (529.6 eV) and structural water (533.9 eV).

The scanning electron microscopy (SEM) image of pure Co foil (Fig. S1, ESI†) indicates that it has a smooth surface structure. The SEM images of $CoC_2O_4·2H_2O$ NA/CF indicate that the entire surface of Co foil is completely covered by $CoC_2O_4·2H_2O$ nanorods array after *in situ* electrodeposition (Fig. 2a). We also investigated the formation processes and morphology changes for $CoC_2O_4·2H_2O$ under different conditions. Fig. S2 (ESI†) shows the SEM images of $CoC_2O_4·2H_2O$ synthesized by the *in situ* electrochemical topotactic conversion method by varying the potentials and reaction times. The side-viewed SEM images (Fig. S3, ESI†) show that the prepared $CoC_2O_4·2H_2O$ structures are generally presented as rod-shaped, which increase in thickness and length with an increase in reaction time. Interestingly, the resultant Co_3O_4 NA/CF still maintains its nanoarray feature (Fig. 2b). The transmission electron microscopy (TEM) image demonstrates that Co_3O_4 nanorod has smooth surface with diameter of about 400 nm (Fig. 2c). The high-resolution TEM (HRTEM) image of a nanorod on Co_3O_4 branches shows a set of lattice spacings of 2.43 Å, which corresponds to the (311) crystallographic plane (Fig. 3b)[25] and is consistent with the selected area electron diffraction (SAED) pattern (inset), suggesting that the cubic Co_3O_4 nanorod structure is dominated by

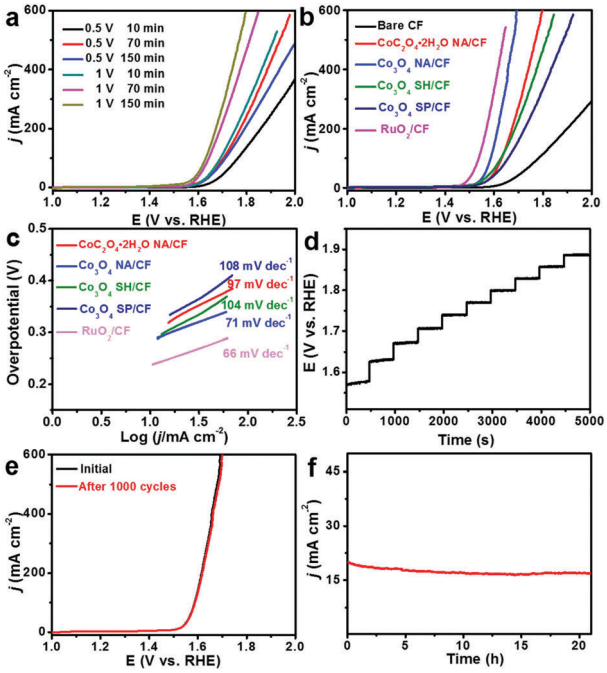

Fig. 3 (a) LSV curves for $CoC_2O_4·2H_2O$ NA/CF at different reaction parameters without *iR* correction. (b) LSV curves for RuO_2/CF, Co_3O_4 NA/CF, $CoC_2O_4·2H_2O$ NA/CF and bare Co with a scan rate of 5 mV s^{-1}. (c) The corresponding Tafel plots for RuO_2/CF, Co_3O_4 NA/CF, $CoC_2O_4·2H_2O$ NA/CF and bare Co. (d) Multi-current process of Co_3O_4 NA/CF. The current density started at 40 mA cm^{-2} and ended at 440 mA cm^{-2}, with an increment of 40 mA cm^{-2} per 500 s without *iR* correction. (e) LSV curves for Co_3O_4 NA/CF before and after 1000 cyclic voltammetry scanning with a scan rate of 100 mV s^{-1}. (f) Time-dependent current density curve at a fixed overpotential of 316 mV. All experiments were carried out in 1.0 M KOH.

[110] crystal orientation.[28,29] Moreover, it can be observed that the Brunauer–Emmett–Teller (BET) surface area of Co_3O_4 NA (75.49 m^2 g^{-1}) is higher than that of $CoC_2O_4·2H_2O$ NA (30.61 m^2 g^{-1}) (Fig. S4a, ESI†). In addition, one peak centered at ~3 nm is detected in the pore size distribution curve of Co_3O_4

NA (Fig. S4b, ESI†), resulting in more exposed sites for the electrocatalysis, which are beneficial for the performance of the OER. All of these results strongly support the successful development of Co_3O_4 nanorods array.

The electrocatalytic water oxidation activity of Co_3O_4 NA/CF (loading: 1.9 mg cm^{-2}) was evaluated by linear scan voltammetry (LSV) using a typical three-electrode system with a scan rate of 5 mV s^{-1} in 1.0 M KOH. The influence of potential and reaction time was also investigated. As presented in Fig. 3a, the results show that $CoC_2O_4{\cdot}2H_2O$ NA/CF (at 1.0 V for 150 min) has optimal OER activity. To directly reflect the intrinsic behavior of catalysts through as-measured reaction currents, the *iR* correction was applied to eliminate the effect of ohmic resistance unless particularly stated.[30–32] RuO_2 on Co foil (RuO_2/CF, loading: 1.9 mg cm^{-2}), Co_3O_4 spheres on Co foil (Co_3O_4 SP/CF, loading: 1.9 mg cm^{-2}), Co_3O_4 sheets on Co foil (Co_3O_4 SH/CF, loading: 1.9 mg cm^{-2}), $CoC_2O_4{\cdot}2H_2O$ NA/CF, and bare Co were also examined for comparison. Fig. 3b shows the LSV curves on a reversible hydrogen electrode (RHE) scale. Clearly, RuO_2/CF exhibits excellent water oxidation activity, while bare Co has poor catalytic activity. Co_3O_4 NA/CF also exhibits much superior catalytic activity with the need of overpotential as low as 308 mV to drive 15 mA cm^{-2}, which are 20, 24 and 14 mV less than that for $CoC_2O_4{\cdot}2H_2O$ NA/CF, Co_3O_4 SP/CF, and Co_3O_4 SH/CF, respectively. In addition, it should be noted that Co_3O_4 NA/CF compares favorably to the OER behavior of most reported materials-derived Co_3O_4 catalysts under alkaline conditions, including C doped Co/Co_3O_4 hollow spheres ($\eta_{15\ mA\ cm^{-2}}$ = 473 mV),[16] Co_3O_4 nanocrystal/carbon paper ($\eta_{15\ mA\ cm^{-2}}$ = 350 mV),[17] RuO_2/Co_3O_4 heterojunctions ($\eta_{10\ mA\ cm^{-2}}$ = 305 mV),[18] hierarchically porous Co_3O_4 ($\eta_{3\ mA\ cm^{-2}}$ = 346 mV),[19] Au@Co_3O_4 core–shell ($\eta_{25\ mA\ cm^{-2}}$ = 370 mV)[33] and $Cu_xCo_{3-x}O_4$ nanoparticles ($\eta_{100\ mA\ cm^{-2}}$ = 367 mV).[34] A more detailed comparison is listed in Table S1 (ESI†). The OER kinetics is also estimated by the corresponding Tafel plots (Fig. 3c). The Tafel slope for Co_3O_4 NA/CF is 71 mV dec^{-1}, which is smaller than that of $CoC_2O_4{\cdot}2H_2O$ NA/CF (97 mV dec^{-1}), Co_3O_4 SP/CF (108 mV dec^{-1}), and Co_3O_4 SH/CF (104 mV dec^{-1}), implying more rapid catalytic kinetics on Co_3O_4 NA/CF electrode. Fig. 3d shows the multi-step chronopotentiometric curve for Co_3O_4 NA/CF with the current density increasing from 40 to 440 mA cm^{-2} (40 mA cm^{-2} per 500 s). The potential immediately levels off at 1.58 V at the start current value and remains unchanged for the remaining 500 s. All other steps exhibit similar results, demonstrating the excellent conductivity, mass transportation and mechanical robustness of 1D Co_3O_4 NA/CF electrode.[35,36] To further reflect charge-transfer rate and catalytic kinetics of electrodes, we also measured the electrochemical impedance spectroscopies (EIS). As shown in Fig. S5 (ESI†), Co_3O_4 NA/CF possesses a smaller radius of semicircle than that for $CoC_2O_4{\cdot}2H_2O$ NA/CF, implying lower R_{ct} and thus a higher charge-transfer rate and faster catalytic kinetics on Co_3O_4 NA/CF.[37–39] Electrochemical durability is another critical factor to evaluate the performance of the catalyst.[40,41] After 1000 cyclic voltammetry cycles, the LSV curves show negligible loss in current density compared with the initial cycle (Fig. 3e). The time-dependent current density curve at fixed overpotential of 316 mV (Fig. 3f) suggests that Co_3O_4 NA/CF can maintain its catalytic activity for at least 22 h, promising its practical applications.

To calculate the electrochemically active surface area of Co_3O_4 NA/CF and $CoC_2O_4{\cdot}2H_2O$ NA/CF electrodes, we applied the double layer capacitance (C_{dl}) at the solid/liquid interface by cyclic voltammetry technique.[42] As shown in Fig. S6a and b (ESI†), the cyclic voltammograms (CVs) were performed in the region of −0.35 to −0.25 V *vs.* Hg/HgO, in which the current responses should only be related to the double layer charging and recharging. The C_{dl} of Co_3O_4 NA/CF is calculated to be 1.52 mF cm^{-2} higher than that of $CoC_2O_4{\cdot}2H_2O$ NA/CF (0.82 mF cm^{-2}). This result indicates that Co_3O_4 NA/CF has a larger electrochemical active surface area and thus more exposed active sites.[43,44]

The assessment of TOFs makes it possible to compare the intrinsic activities of different catalysts, and we quantified the surface concentration of active sites by electrochemistry.[45] For TOF calculations, the surface concentration of the active sites associated with the redox Co species needs to be known. It was observed that the oxidation peak current of the redox species shows a linear dependence on the scan rate during electrochemical CV (Fig. 4a and b); the slope is derived from the linear relationship (Fig. 4c). The number of active Co species (m) is calculated using the formula: slope = $n^2F^2m/4RT$ (where n is the numbers of electron transferred; R and T are the ideal gas constant and the absolute temperature, respectively.) The m for Co_3O_4 NA/CF is 2.24 × 10^{-7} mol, which is smaller than that $CoC_2O_4{\cdot}2H_2O$ NA/CF of (1.56 × 10^{-6} mol). Fig. 4d shows the plots of TOF *vs.* overpotentials for $CoC_2O_4{\cdot}2H_2O$ NA/CF and Co_3O_4 NA/CF, suggesting much higher TOFs for Co_3O_4 NA/CF at overpotential of 0.35 V.

Co atoms are regarded as the active centers for OER in Co_3O_4 nanorods. In the CV of Co_3O_4 (Fig. 4b, 20 mV s^{-1}), there are two anodic peaks with corresponding cathodic peaks at lower

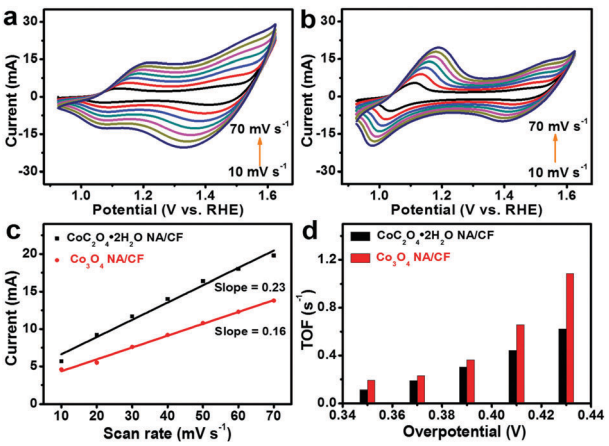

Fig. 4 CVs of (a) Co_3O_4 NA/CF and (b) $CoC_2O_4{\cdot}2H_2O$ NA/CF after OER electrolysis under different scan rates increasing from 10 to 70 mV s^{-1} in 1.0 M KOH. (c) Linear relationship of the oxidation peak currents *vs.* scan rates for Co_3O_4 NA/CF and $CoC_2O_4{\cdot}2H_2O$ NA/CF. (d) TOF comparison between Co_3O_4 NA/CF and $CoC_2O_4{\cdot}2H_2O$ NA/CF at different fixed overpotentials.

potential. According to the Pourbaix diagram (pH = 14), the peak at 1.14 V is assigned to the oxidation of Co^{2+} and Co^{3+}, and the peak at 1.49 V implies the further oxidation of Co^{3+} and Co^{4+}. Moreover, Fig. S7 (ESI†) shows a scheme of the proposed OER mechanism on Co_3O_4. After oxidation of Co_3O_4, the obtained Co^{3+} compound CoOOH is constructed by octahedral $Co^{3+}O_6$ and the surface is terminated by Co^{3+}–OH. The further oxidized Co^{4+}–O species are found to be the active species for the OER, and they couple with one of the neighboring O atoms, resulting in the formation of an O–O bond belonging to a hydroperoxo Co^{4+}–OOH or to a peroxo Co^{4+}–OO species. Finally, the O_2 molecule is released and the catalyst converts back to Co^{3+}. Therefore, the net reaction can be written as $4OH^- \rightarrow 2H_2O + 4e^- + O_2$.[31]

In summary, *in situ* electrochemical conversion is proven to be an effective strategy toward development of Co_3O_4 nanorods array with high conductivity. As a 1D catalyst electrode, the Co_3O_4 NA/CF shows superior activity toward water oxidation needing overpotential of 308 mV to drive a geometrical catalytic current density of 15 mA cm^{-2} in 1.0 M KOH with good long-term electrochemical durability and a high TOF (0.646 mol s^{-1}, η = 410 mV). This study not only provides us an attractive low-cost catalyst material for efficient and durable electrochemical water oxidation in alkaline media, but opens up an exciting new avenue to the rational design and fabrication of transition metal oxides based nanoarrays for applications in electrocatalysis.

This work was supported by the National Natural Science Foundation of China (No. 21775054, 21601064, 21575050), the National Key Scientific Instrument and Equipment Development Project of China (No. 21627809), the Taishan Scholar Foundation of Shandong Province (No. ts20130937) and Natural Science Foundation of Shandong Province (No. ZR2016JL013 and ZR2016BQ10).

Conflicts of interest

There are no conflicts to declare.

References

1 J. Chow, R. J. Kopp and P. R. Portney, *Science*, 2003, **302**, 1528–1531.
2 R. F. Service, *Science*, 2009, **324**, 1257–1259.
3 M. S. Dresselhaus and I. L. Thomas, *Nature*, 2001, **414**, 332.
4 Q. Yin, J. M. Tan, C. Besson, Y. V. Geletii, D. G. Musaev, A. E. Kuznetsov, Z. Luo, K. I. Hardcastle and C. L. Hill, *Science*, 2010, **328**, 342–345.
5 Q. Liu, L. Xie, Z. Liu, G. Du, A. M. Asiri and X. Sun, *Chem. Commun.*, 2017, **53**, 12446–12449.
6 Y. Lee, J. Suntivich, K. J. May, E. E. Perry and Y. J. Shao-Horn, *J. Phys. Chem. Lett.*, 2012, **3**, 399–404.
7 J. Wang, W. Cui, Q. Liu, Z. Xing, A. M. Asiri and X. Sun, *Adv. Mater.*, 2016, **28**, 215–230.
8 L. Xie, C. Tang, K. Wang, G. Du, A. M. Asiri and X. Sun, *Small*, 2017, **13**, 1602755.
9 X. Zou and Y. Zhang, *Chem. Soc. Rev.*, 2015, **44**, 5148–5180.
10 L. Han, S. Dong and E. Wang, *Adv. Mater.*, 2016, **28**, 9266–9291.
11 M. Hamdani, R. N. Singh and P. Chartier, *Int. J. Electrochem. Sci.*, 2010, **5**, 556–577.
12 L. Hu, Q. Peng and Y. Li, *J. Am. Chem. Soc.*, 2008, **130**, 16136–16137.
13 Z. Zhang, J. Hao, W. Yang, B. Lu, X. Ke, B. Zhang and J. Tang, *ACS Appl. Mater. Interfaces*, 2013, **5**, 3809–3815.
14 Y. Zhu, T. Ma, M. Jaroniec and S. Qiao, *Angew. Chem., Int. Ed.*, 2017, **56**, 1324–1328.
15 X. Liu, J. Jiang and L. Ai, *J. Mater. Chem. A*, 2015, **3**, 9707–9713.
16 L. Hang, Y. Sun, D. Men, S. Liu, Q. Zhao, W. Cai and Y. Li, *J. Mater. Chem. A*, 2017, **5**, 11163–11170.
17 S. Du, Z. Ren, J. Zhang, J. Wu, W. Xi, J. Zhu and H. Fu, *Chem. Commun.*, 2015, **51**, 8066–8069.
18 H. Liu, G. Xia, R. Zhang, P. Jiang, J. Chen and Q. Chen, *RSC Adv.*, 2017, **7**, 3686–3694.
19 L. Yao, H. Zhong, C. Deng, X. Li and H. Zhang, *J. Energy Chem.*, 2016, **25**, 153–157.
20 W. Hong, C. Shang, J. Wang and E. Wang, *Energy Environ. Sci.*, 2015, **8**, 2910–2915.
21 W. Hong, J. Wang and E. Wang, *Small*, 2014, **10**, 3262–3265.
22 W. Hong, J. Wang and E. Wang, *Nanoscale*, 2016, **8**, 4927–4932.
23 W. Hong, J. Wang and E. Wang, *J. Mater. Chem. A*, 2015, **3**, 13642–13647.
24 W. Hong, J. Wang and E. Wang, *Nano Res.*, 2015, **8**, 2308–2316.
25 L. Ren, P. Wang, Y. Han, C. Hu and B. Wei, *Chem. Phys. Lett.*, 2009, **476**, 78–83.
26 L. Xu, Z. Wang, J. Wang, Z. Xiao, X. Huang, Z. Liu and S. Wang, *Nanotechnology*, 2017, **28**, 165402.
27 L. Xu, Q. Jiang, Z. Xiao, X. Li, J. Huo, S. Wang and L. Dai, *Angew. Chem., Int. Ed.*, 2016, **55**, 5277–5281.
28 X. Xie, Y. Li, Z. Liu, M. Haruta and W. Shen, *Nature*, 2009, **458**, 746.
29 Y. Sun, R. Xu, J. Yang, L. He, J. Nie, R. Dou, W. Zhou and L. Guo, *Nanotechnology*, 2010, **21**, 335605.
30 W. Lu, T. Liu, L. Xie, C. Tang, D. Liu, S. Hao, F. Qu, G. Du, Y. Ma, A. M. Asiri and X. Sun, *Small*, 2017, **13**, 1700805.
31 C. Tang, L. Xie, X. Sun, A. M. Asiri and Y. He, *Nanotechnology*, 2016, **27**, 20LT02.
32 Q. Liu, L. Xie, F. Qu, Z. Liu, G. Du, A. M. Asiri and X. Sun, *Inorg. Chem. Front.*, 2017, **4**, 1120–1124.
33 Z. Zhuang, W. Sheng and Y. Yan, *Adv. Mater.*, 2014, **26**, 3950–3955.
34 X. Wu and K. Scott, *J. Mater. Chem.*, 2011, **21**, 12344–12351.
35 M. Xie, L. Yang, Y. Ji, Z. Wang, X. Ren, Z. Liu, A. M. Asiri, X. Xiong and X. Sun, *Nanoscale*, 2017, **9**, 16612–16615.
36 F. Xie, H. Wu, J. Mou, D. Lin, C. Xu, C. Wu and X. Sun, *J. Catal.*, 2017, **356**, 165–172.
37 X. Ren, D. Wu, R. Ge, X. Sun, H. Ma., T. Yan, Y. Zhang, B. Du, Q. Wei and L. Chen, *Nano Res.*, 2017, DOI: 10.1007/s12274-017-1818-6.
38 J. Zhao, X. Ren, H. Ma, X. Sun, Y. Zhang, T. Yan, Q. Wei and D. Wu, *ACS Sustainable Chem. Eng.*, 2017, **5**, 10093–10098.
39 X. Xiong, Y. Ji, M. Xie, C. You, L. Yang, Z. Liu, A. M. Asiri and X. Sun, *Electrochem. Commun.*, 2018, **86**, 161–165.
40 X. Ren, R. Ge, Y. Zhang, D. Liu, D. Wu, X. Sun, B. Du and Q. Wei, *J. Mater. Chem. A*, 2017, **5**, 7291–7294.
41 X. Ren, W. Wang, R. Ge, S. Hao, F. Qu, G. Du, A. M. Asiri, Q. Wei, L. Chen and X. Sun, *Chem. Commun.*, 2017, **53**, 9000–9003.
42 S. Trasatti and O. A. Petrii, *J. Electroanal. Chem.*, 1992, **327**, 353–376.
43 D. Wu, Y. Wei, X. Ren, X. Ji, Y. Liu, X. Guo, Z. Liu, A. M. Asiri, Q. Wei and X. Sun, *Adv. Mater.*, 2018, 1705366.
44 X. Ren, Y. Ji, Y. Wei, D. Wu, Y. Zhang, M. Ma, Z. Liu, A. M. Asiri, Q. Wei and X. Sun, *Chem. Commun.*, 2018, DOI: 10.1039/c7cc08748a.
45 M. Ma, F. Qu, X. Ji, D. Liu, S. Hao, G. Du, A. M. Asiri, Y. Yao, L. Chen and X. Sun, *Small*, 2017, **13**, 1700394.

